

Cite this: *Chem. Sci.*, 2024, **15**, 14336

All publication charges for this article have been paid for by the Royal Society of Chemistry

Self-correcting mismatches in metastable hydrogen-bonded organic frameworks with an 11-fold interpenetrated array†

Guomin Xia, ^{‡bc} Chunlei Zhou, ^c Xingliang Xiao, ^{bc} Yang Yang, ^{bc} Fuqing Yu, ^{ab} and Hongming Wang ^{*abc}

The polymorphic self-correction from a metastable phase to a stable one often occurs and plays crucial roles in synthesizing robust hydrogen-bonded organic frameworks (HOFs). However, identifying metastable phases and understanding the self-correcting mechanisms is a challenging venture due to their intrinsic instability. Here, we for the first time introduce 1,8-naphtholactam (Np) as a hydrogen-bonding synthon positioned on the periphery of a carbazole to create a versatile molecular unit for 3D HOFs. The as-synthesized NCU-HOF1, analyzed by single-crystal X-ray diffraction (SCXRD), is found to be metastable. It exhibits an 11-fold interpenetrated dia topology with a quarter of the Np units exhibiting monomeric N-H···O interactions between adjacent Np link sites, which readily self-correct upon desolvation to form fully dimeric ones. Consequently, the resultant NCU-HOF1a becomes highly robust in polar solvents, strong acid or alkaline aqueous solutions, and has permanent porosity with contracted cavities for selective adsorption and efficient "turn-up" fluorescent sensing of C₂H₄ gas. This work not only debuts a new hydrogen-bonding synthon but offers more insights into investigating solid-state dynamics in metastable HOFs.

Received 25th April 2024
Accepted 5th August 2024

DOI: 10.1039/d4sc02751e
rsc.li/chemical-science

Introduction

Hydrogen-bonded organic frameworks (HOFs) represent a rapidly evolving class of synthetic crystalline porous materials with substantial potential spanning diverse scientific disciplines.^{1–7} Their distinctive attributes, encompassing porosity, tunability, sustainability, and practicality, render them compelling candidates for a myriad of applications, including gas adsorption and separation,^{8–10} proton conduction,^{11,12} heterogeneous catalysis,^{13,14} biomedical applications,^{15–17} and beyond. Generally, HOFs are self-assembled by the interaction of organic molecule units through non-covalent hydrogen-bonds.^{18,19} In this regard, the carboxylic acid,^{20–22} diamino-triazine (DAT),^{23,24} pyrazole,^{25,26} imidazole,^{27,28} benzimidazolone,^{29,30} and charge-assisted ionic hydrogen bonding patterns^{31–33} have been employed in constructing HOF archetypes. In the past decade, careful selection of building blocks

and functional group modifications within specific organic molecular units have led to significant advancements in the geometry of HOFs. These advancements encompass aspects such as shape, size, symmetry, and dimensions, as well as surface chemistry^{1–5,34–40} underscoring the crucial role of pre-design strategies.

However, the exploration of HOFs has presented a substantial challenge in implementing reticular chemistry for the self-assembly of hydrogen-bonding units. Hydrogen bonds exhibit significantly weaker (10–40 kJ mol^{–1}), more flexible, and less directional bonding energies and angles compared to coordination (90–350 kJ mol^{–1}) and covalent bonds (300–600 kJ mol^{–1}).^{1,41} These intrinsic characteristics of hydrogen bonds in HOFs enable mild synthesis conditions,^{42,43} solution processability,^{42,44} and ease of regeneration,^{45,46} yet simultaneously result in the facile formation of metastable structures and complexity.^{47–49} The arrangement of hydrogen bonds among organic molecule units is susceptible to disruption by solvent disturbances, leading to the formation of (non)porous networks. These networks typically exhibit undesired hydrogen bonding between donor and acceptor groups, as well as fractured hydrogen bonds interacting with solvent molecules.^{50–54} This situation would be aggravated within highly interpenetrated HOFs, where the interpenetration of frameworks promotes synergistic interactions (π – π stacking, Ar/C–H··· π interactions, van der Waals interactions)^{18,55,56} among organic molecule units to further stabilize these mismatched hydrogen

^aCollege of Chemistry and Chemical Engineering, Nanchang University, Nanchang 330031, China. E-mail: hongmingwang@ncu.edu.cn

^bJiangxi Provincial Key Laboratory of Functional Crystalline Materials Chemistry, Nanchang 330031, China. E-mail: guominxia@ncu.edu.cn

^cInstitute for Advanced Study, Nanchang University, Nanchang 330031, China

† Electronic supplementary information (ESI) available. CCDC 2226443–2226446. For ESI and crystallographic data in CIF or other electronic format see DOI: <https://doi.org/10.1039/d4sc02751e>

‡ These authors contributed equally to this work.



bonds. It is thus believed that investigating the solid-state dynamics of mismatched hydrogen bond patterns within metastable HOFs would contribute to deeply deciphering their self-assembly and evolution, yet it remains an ongoing dilemma.

In this study, we fabricated 3D HOFs by the self-assembly of organic molecule units consisting of peripheral 1,8-naphtholactam (Np) and central bicarbazole in solution. The selection of the Np synthon was based on its fluorescence behaviors and its capacity to form stable dimers through intermolecular hydrogen bonding, as recently reported in our laboratory.^{57,58} Utilizing single-crystal X-ray diffraction (SCXRD) data, we present, for the first time, the self-correcting mismatches of hydrogen bond patterns in an 11-fold interpenetrated array of metastable HOF1 upon desolvation (Fig. 1). This involved a remarkable “cross-door” rotation of nearly 180° between adjacent frameworks at the Np link sites with monomeric N–H···O interactions. The ensuing permanent porosity with contracted cavities, coupled with structural robustness and bright green emission of the activated NCU-HOFs were then illustrated, enabling the selective adsorption and efficient “turn-up” fluorescent sensing of ethylene (C₂H₄) gas.

Results and discussion

The organic ligand BC-4Np was synthesized through a Suzuki coupling reaction involving 3,3',6,6'-tetrabromo-9,9'-bicarbazole (BC-4Br) and boric acid esterified Np (Np-pin). Comprehensive characterization of its molecular structure was achieved using ¹H NMR, ¹³C NMR, and mass spectroscopy, yielding satisfactory results (details in the ESI†). Block-shaped single crystals were obtained *via* vapor diffusion of acetone into a solution of BC-4Np in *N,N'*-dimethylformamide (DMF) at 298 K. SCXRD analysis disclosed that NCU-HOF1 crystallizes in the monoclinic space group *I*2/*a* (Table S1†). Within NCU-HOF1, two crystallographically unique BC-4Np molecules exist in the asymmetric unit (Fig. 2a). Distinct hydrogen bonding modes between adjacent Np linkers were observed within each BC-4Np unit, featuring partially monomeric and fully dimeric N–H···O hydrogen bonds in a 1 : 2 ratio, with distances ranging from 1.89

to 2.04 Å, forming a single dia 3D network (Fig. 2b). The substantial void space of 70.4 × 49.4 Å² in this single dia 3D network facilitates the formation of a dia{6⁶} topological structure with an 11-fold interpenetrated array (Fig. 2c and d). This interpenetration is primarily facilitated by multiple Ar–H···O, Ar–H···π, and π–π interactions between Np and adjacent BC/Np moieties in BC-4Np units (Fig. S1 and S2†). These observations underscore the pivotal role of the large π-planar configuration of the Np synthon in the highly interpenetrated array of NCU-HOF1. Despite the 11-fold interpenetration, serrated 1D pore channels along the *c*-axis in NCU-HOF1 persist, with cages measuring 9.0 × 9.6 Å² and necks as small as 5.3 Å (type I, Fig. S3†). Additionally, isolated cavities with cross-sections of approximately 7.6 × 7.0 Å² were detected in NCU-HOF1 (type II, Fig. S3†). The total solvent-accessible void of NCU-HOF1 was estimated to be around 30% using PLATON.⁵⁹

During the activation process, a noteworthy phenomenon was observed in the desolvation of the as-synthesized sample (NCU-HOF1) under high vacuum to generate the activated sample (NCU-HOF1a). The powder X-ray diffraction (PXRD) patterns displayed significant changes, including a shift in the strongest diffraction peak of NCU-HOF1 from 3.1° to 5.2° and a reduction in the number of diffraction peaks, indicative of a structural transformation during desolvation (Fig. S4†). Subsequent tests revealed that elevated temperature and/or vacuum conditions induced a phase transition in NCU-HOF1 (Fig. 3a). Variable-temperature PXRD patterns demonstrated that the phase transition occurred at 313 K, despite being degenerate (Fig. 3b). This observation was corroborated by thermogravimetric analysis (TGA) and differential scanning calorimetry (DSC) data under nitrogen (N₂) conditions (Fig. S5†), suggesting the facile escape of disordered solvent molecules from the frameworks. Fourier transform infrared spectroscopy (FTIR) further indicated the structural transformation of NCU-HOF1, as evidenced by the disappearance of the absorption peak at 1713 cm⁻¹, establishing a close correlation with the hydrogen bond receptor C=O in Np synthons (Fig. 3c).

Through acetone immersion and vacuum outgassing at 298 K, the guest-free NCU-HOF1a crystal structure is successfully obtained for X-ray diffraction analysis, employing a single-crystal-to-single-crystal (SCSC) transformation approach. SCXRD analysis reveals that NCU-HOF1a crystallizes in the monoclinic space group *C*2/*c*, maintaining an 11-fold interpenetrated array with a slight lattice volume contraction in the same dia topology (Table S1 and Fig. S6 and S7†). In contrast to the metastable NCU-HOF1, all BC-4Np molecules in NCU-HOF1a exhibit higher structural symmetry and become crystallographically equivalent. This transformation is associated with the conversion of N–H···O interactions between adjacent Np link sites from being partially monomeric to completely dimeric upon activation (Fig. 3d). This observation aligns with the (FTIR) data, underscoring the significance of the hydrogen-bonding pattern in this self-correcting process. A detailed analysis reveals a “cross-door” rotation of two Np units in A-A layers, reaching an angle of nearly 180° (Fig. S8†). Simultaneously, two BC-4Np molecules at the adjacent B layer slide

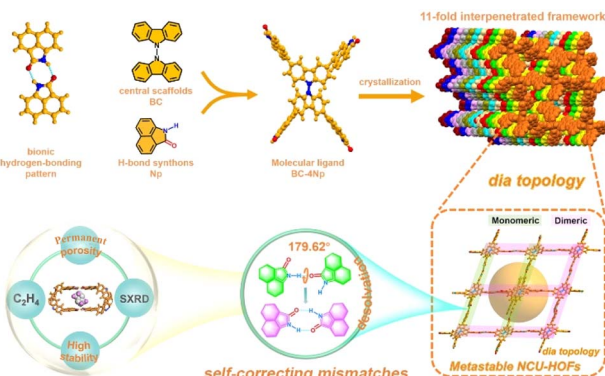


Fig. 1 Schematic diagram illustrating the self-correcting mismatches within NCU-HOFs constructed from the BC-4Np molecular ligand.



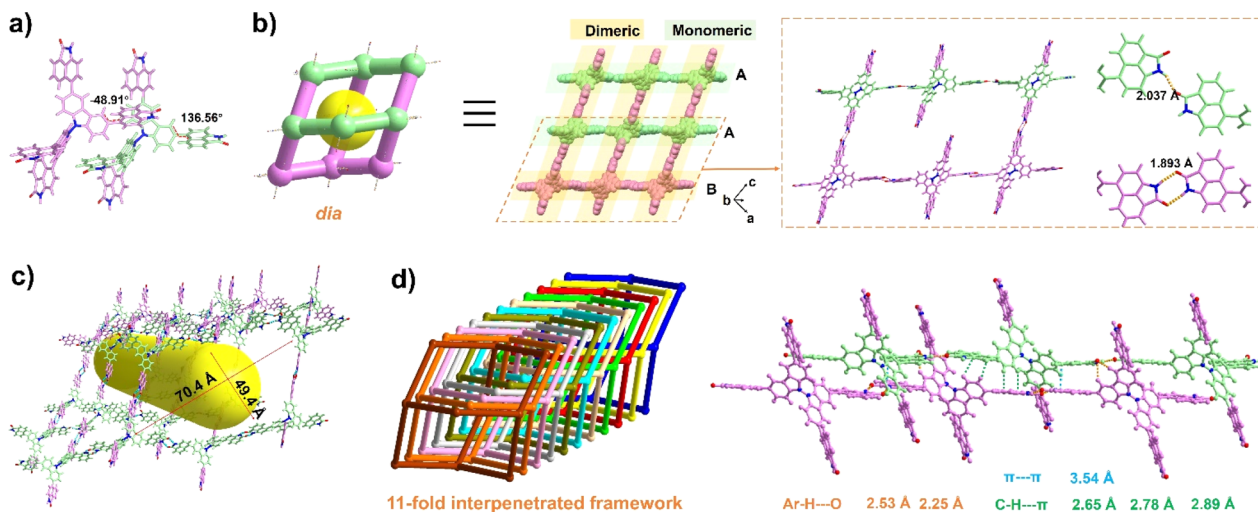


Fig. 2 (a) Distinct molecular configurations of BC-4Np. (b) Alternating monomeric and dimeric N-H...O hydrogen bonds between adjacent BC-4Np molecules. (c) Void space in the dia topology in NCU-HOF1. (d) The 11-fold interpenetrated topological frameworks (different colors represent different frameworks) and side view of the stacking. The purple structure represents the dimer formed, and the mint green one represents the monomer.

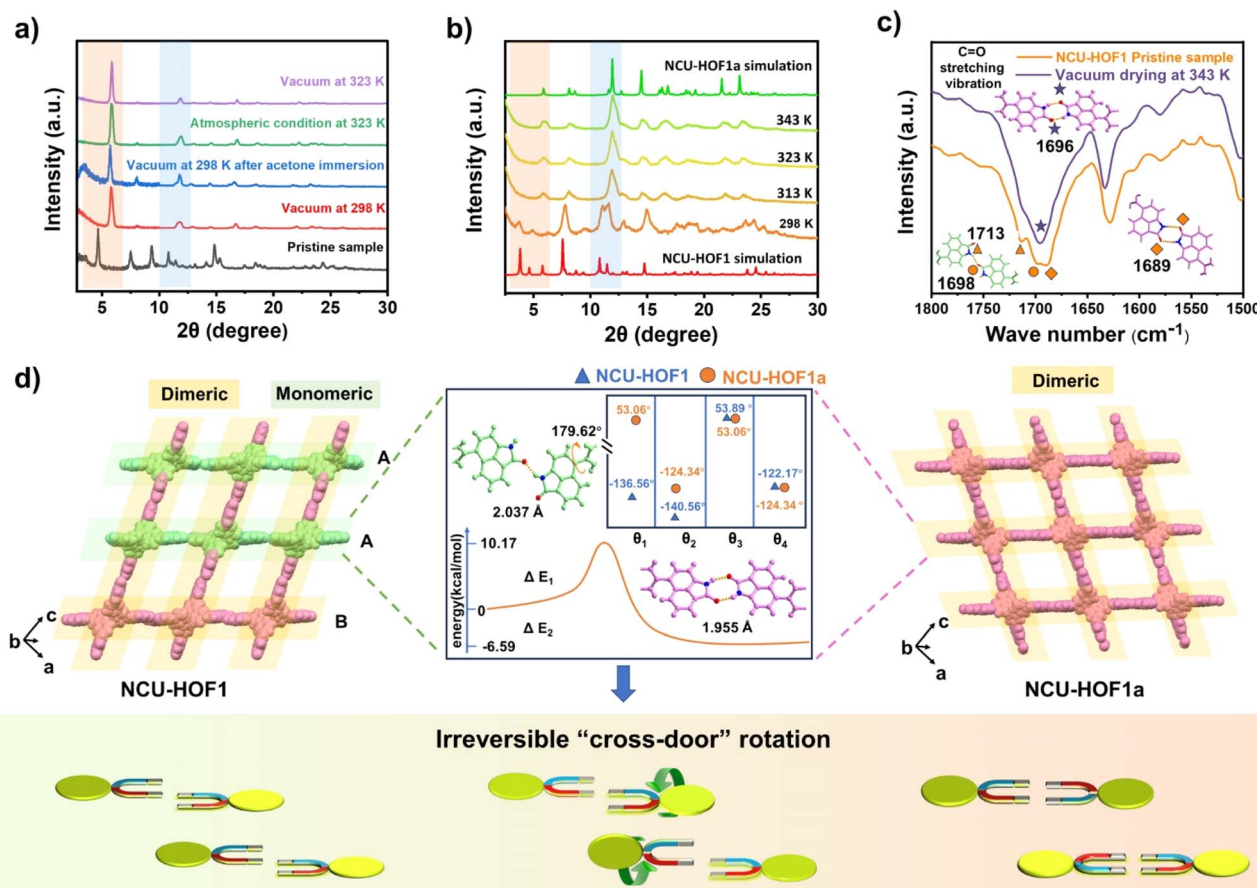


Fig. 3 (a) PXRD variations of NCU-HOF1 upon desolvation (vacuum: -1 bar). (b) Variable-temperature PXRD patterns of degraded NCU-HOF1 under a N_2 atmosphere. (c) *In situ* FTIR spectrum of NCU-HOF1. (d) Schematic diagram illustrating the self-correcting N-H...O interactions between adjacent Np link sites through an irreversible "cross-door" rotation pathway. Inset: The difference in dihedral angles between the carbazole and Np segments, and the energy profile from monomer to dimer formation of BC-4Np in NCU-HOF1.



towards each other in opposite directions, maintaining a distance of approximately 4.6 Å. This sliding is primarily induced by the C-H···O interaction between the neighboring Np units at layers A and B, generating π -stacking in the frameworks. The self-correction dynamics, characterized by a dramatic rotation and slip of assembly units within the 11-fold interpenetrated HOFs, represent a remarkable and hitherto unreported phenomenon.

In the context of energy considerations, the transformation of monomeric Np units into dimers occurs through rotation around the N-H···O bond, exhibiting an energy barrier of 10.17 kcal mol⁻¹ and an exothermic process of 6.57 kcal mol⁻¹ (Fig. 3d middle). When the free N-H of Np units is stabilized by guest acetone molecules, rotation becomes unlikely due to the presence of a higher energy barrier of 28.30 kcal mol⁻¹ and an exothermic energy of 5.79 kcal mol⁻¹ (Fig. S9†). The theoretical analysis concurs with the experimental observation that NCU-HOF1 can be easily activated into NCU-HOF1a through heating and/or vacuum conditions, as it removes guest acetone molecules. Following activation, the serrated 1D pore channel of the HOFs contracts into a dispersive 0D pore, resulting in a reduction of the void pore volume to approximately 20%. Furthermore, NCU-HOF1a crystals exhibit two types of irregular cavities (I and II), primarily surrounded by Np synthons (Fig. 4a). Along the *c*-axis, cavity I features the largest cages measuring 5.5 × 5.6 Å² with the smallest necks of 3.7 Å, while cavity II comprises cages of 5.3 × 7.2 Å² with the smallest necks of 3.5 Å (Fig. S10†). These dimensions align more favorably with

the size of small C₂H₄ molecules (3.3 × 4.2 × 4.8 Å³) than ethane (C₂H₆) molecules (3.8 × 4.1 × 4.8 Å³),⁸ providing additional motivation for exploring potential capture and separation within these contracted cavities.

To assess chemical stability, NCU-HOF1a underwent treatment in common organic solvents (methanol, acetonitrile, acetone, trichloromethane, and toluene), HCl (pH = 1), and NaOH (pH = 13) solutions at 298 K. After one month, the framework retained its structural integrity, as confirmed by PXRD patterns, scanning electron microscope (SEM) images, and fluorescence photographs (Fig. S11 and S12†), revealing its high structural robustness. Variable-temperature PXRD patterns demonstrated NCU-HOF1a's exceptional thermal stability, with the decomposition temperature confirmed to be above 578 K by thermogravimetric analysis in an N₂ atmosphere (Fig. S13†). It is noteworthy that the conversion of NCU-HOF1a to NCU-HOF1 could not be achieved, even when soaked in the mother solution for sample preparation, confirming its thermodynamic stability (Fig. S14†). This irreversibility aligns with crystallographic data both before and after the structural transformation, underscoring the self-correction of the mismatched hydrogen-bonding pattern. Meanwhile, NCU-HOF1a exhibited a maximum emission wavelength (λ_{em}) at 526 nm with a fluorescence quantum yield (Φ_{PL}) of up to 36.1% (Fig. S15†). The bright yellow fluorescence of NCU-HOF1a remained unchanged after immersion in common organic solvents and strong acid or alkali water solutions. The fluorescence decay profiles fit well with a double-exponential function,

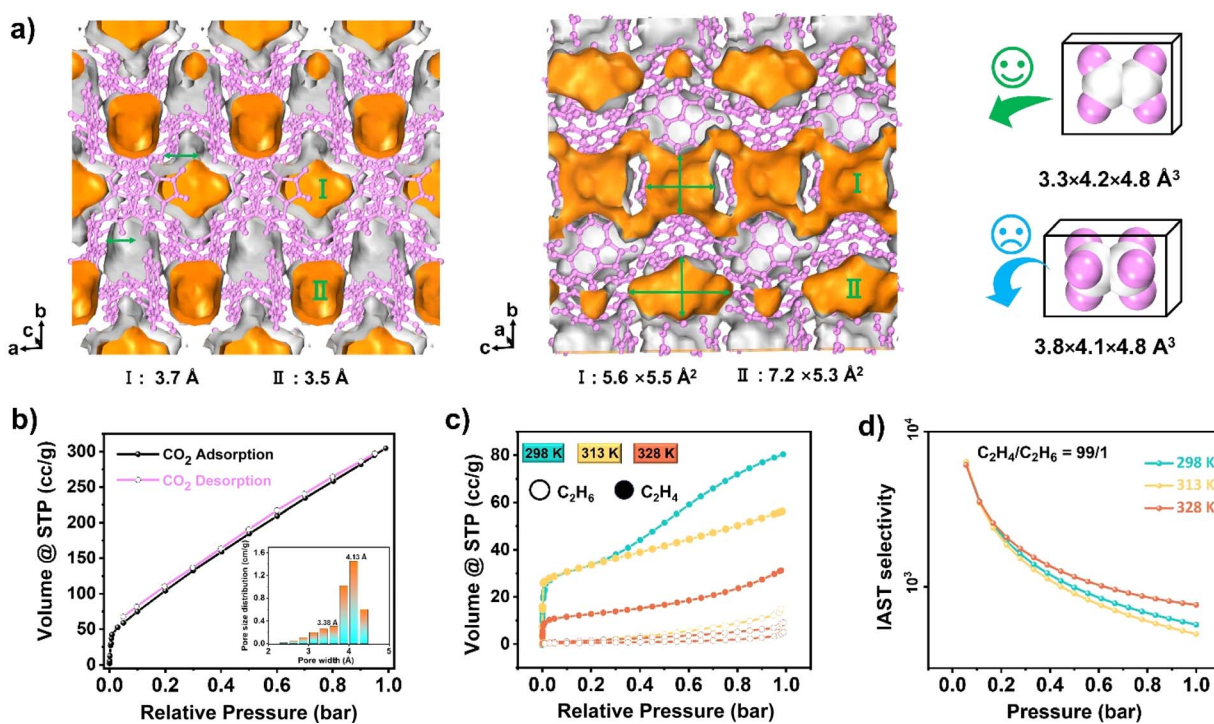


Fig. 4 (a) Framework with two pore channels in NCU-HOF1a and the schematic diagram of the size-dependent separation for C₂H₄ and C₂H₆ molecules. (b) Gas adsorption and desorption curves for CO₂ in NCU-HOF1a at 273 K. (c) Gas adsorption isotherms for C₂H₄ (hollow circles) and C₂H₆ (solid circles) in NCU-HOF1a at 298 K (cyan), 313 K (orange), and 333 K (dull red). (d) IAST selectivity of NCU-HOF1a for C₂H₄ (99 : 1, v/v) at 298 K (cyan), 313 K (orange), and 333 K (dull red).



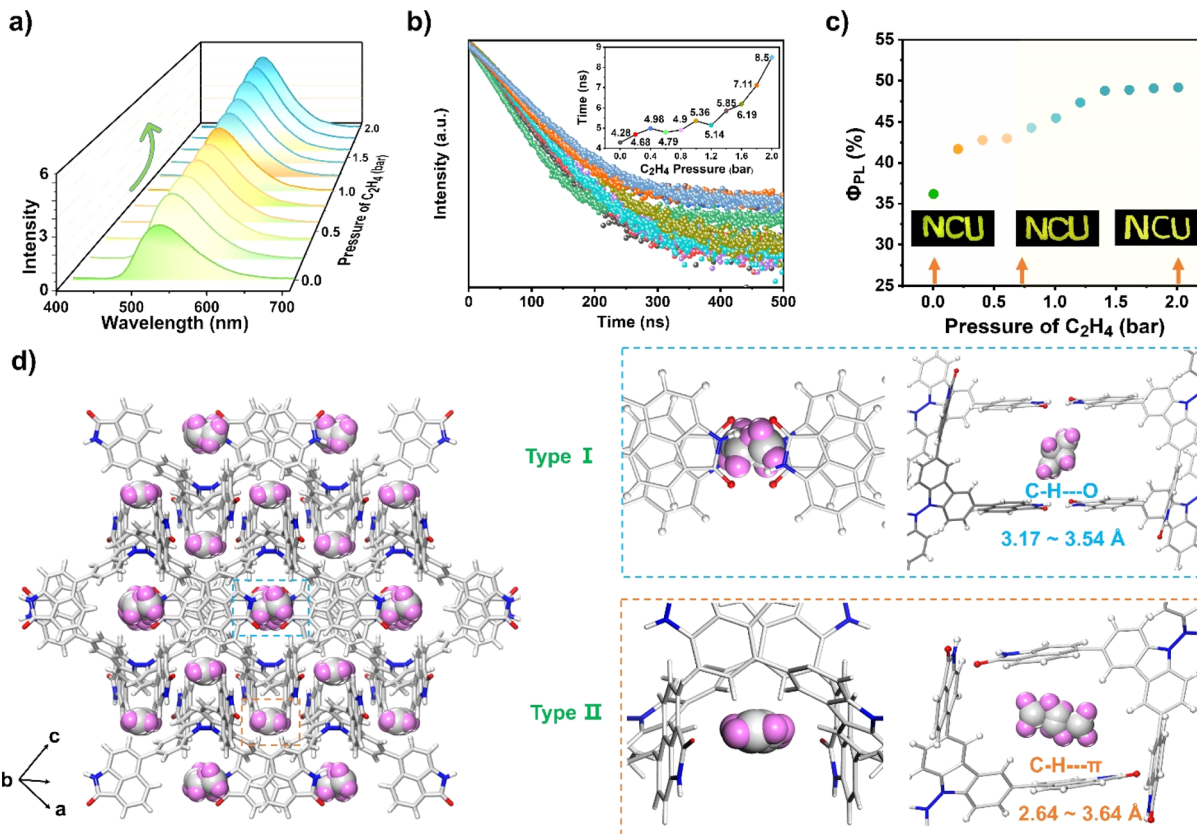


Fig. 5 Changes in (a) fluorescence intensity, (b) lifetime profiles, and (c) Φ_{PL} of NCU-HOF1a upon C_2H_4 uptake (pressure ranging from 0 to 2 bar). (d) Multiple intermolecular interactions between C_2H_4 gas and Np synthons in the framework of NCU-HOF1a.

characterized by short lifetimes of approximately 4.79 ns (Fig. S15†). These fluorescence features, mainly inherited from Np synthons, can be sustained and are highly consistent with chemical stability. Notably, NCU-HOF1a represents the first instance of high-efficiency fluorescence derived from hydrogen-bonding synthons, with fluorescence efficiencies comparable to those reported in previous HOF literature (Table S2†).

The permanent porosity of NCU-HOF1a was established through carbon dioxide (CO_2) gas sorption experiments at 273 K. In Fig. 4b, the adsorbed CO_2 amount in the first step, at $P/P_0 = 0.001$, is approximately $40\text{ cm}^3\text{ g}^{-1}$, indicative of a micropore filling process. The total CO_2 uptake at 1 bar reaches $300\text{ cm}^3\text{ g}^{-1}$, corresponding to a total pore volume of $0.122\text{ cm}^3\text{ g}^{-1}$, consistent with the theoretical value calculated from the crystal structure ($0.103\text{ cm}^3\text{ g}^{-1}$). A small hysteresis loop suggests that HOFs effectively preserve pore characteristics during the adsorption/desorption process. The Brunauer–Emmett–Teller (BET) surface area of NCU-HOF1a was calculated to be $538\text{ m}^2\text{ g}^{-1}$ (Fig. S16†), comparable to reported counterparts with an 11-fold interpenetrated array.⁶⁰ The pore size distribution, calculated using non-localized density functional theory (NL-DFT), exhibited main peaks at 3.38 and 4.13 \AA , consistent with values obtained from the crystal structure using the Poreblazer program (Fig. 4b and S17†). N_2 isotherms at 77 K revealed a characteristic reversible type-III isotherm for NCU-HOF1a

(Fig. S18†), indicating an extremely weak interaction between NCU-HOF1a and N_2 gas.

Single-component adsorption isotherms of C_2H_6 and C_2H_4 for NCU-HOF1a were examined under ambient conditions (Fig. 4c and S19 and Table S3†). The total C_2H_4 uptake at 298 K and 1 bar was $80.93\text{ cm}^3\text{ g}^{-1}$ (3.61 mmol g^{-1}), with a second adsorption step at 0.4 bar indicating dual adsorption sites for C_2H_4 , one of which exhibits preferential adsorption. Conversely, a type-IV isotherm was detected for C_2H_6 adsorption, and the total C_2H_6 uptake was only $14.80\text{ cm}^3\text{ g}^{-1}$ (0.66 mmol g^{-1}) under identical conditions. Such a preferential adsorption of C_2H_4 over C_2H_6 is accompanied by a large adsorption ratio for C_2H_4/C_2H_6 (5.46), suggesting the potential of NCU-HOF1a for separating these two gases. Additionally, the total C_2H_4 uptake decreased with rising temperature, and the second adsorption step vanished at 313 K and 328 K. Calculations of the adsorption selectivity of NCU-HOF1a for C_2H_4/C_2H_6 (50/50, 90/10 and 99/1) mixtures using ideal adsorbed solution theory (IAST) revealed high C_2H_4 selectivity for mixtures at 298 K and 1 bar (Fig. 4d and S20 and Table S3†). The initial value of the experimental isosteric heat of adsorption (Q_{st}) for C_2H_4 on NCU-HOF1a was calculated to be 20 kJ mol^{-1} , indicating superior adsorption/desorption processes compared to traditional metals or π coordination gas adsorbing materials.⁶¹

The fluorescence behavior of NCU-HOF1a before and after C_2H_4 uptake was then recorded. As shown in Fig. 5a–c, the as-



prepared NCU-HOF1a@C₂H₄ (for preparation details see the ESI†) maintained bright yellow-green fluorescence at $\lambda_{\text{em}} = 526$ nm, with Φ_{PL} and lifetime gradually increasing from 36.1 to 49.1% and from 4.28 to 8.50 ns upon C₂H₄ uptake. In comparison, NCU-HOF1a showed a negligible increase in fluorescence intensity upon treatment with C₂H₂ or C₂H₆ gas, emphasizing its exceptional selectivity for C₂H₄ adsorption (Fig. S21†). Variable-temperature fluorescence tests revealed that NCU-HOF1a@C₂H₄ remains structurally stable under ambient conditions but readily releases adsorbed C₂H₄ during vacuum drying (Fig. S22†). This fluorescence enhancement can be repeated at least five times with C₂H₄ pressure ranging from 0 to 2 bar, indicating the excellent reusability of NCU-HOF1a for C₂H₄ uptake/release (Fig. S23a†). The unchanged PXRD pattern of NCU-HOF1a before and after C₂H₄ uptake demonstrated that the adsorbed C₂H₄ gas has no impact on its framework (Fig. S23b†). A summary of all the photophysical data of the as-prepared NCU-HOF1a@C₂H₄ is provided in Table S4.†

Fortunately, the C₂H₄-adsorbed NCU-HOF1a single crystal, named NCU-HOF1a@1C₂H₄, was obtained by exposing it to a C₂H₄ atmosphere at 1 bar and 273 K for approximately 24 hours (Table S1 and Fig. S24 and S25†). With the SCXRD results of NCU-HOF1a@1C₂H₄, the C₂H₄-induced fluorescence enhancement behavior of NCU-HOF1a can be further elucidated. Although the location and configuration of the C₂H₄ molecules within the pores are disordered, two possible modes of C₂H₄ molecules residing in the NCU-HOF1a framework were observed. In Fig. 5d, the C₂H₄ molecules were trapped between multiple Np synthons in NCU-HOF1a@1C₂H₄, forming weak C–H···O interactions (3.17–3.54 Å) in the type-I cavity, while forming moderate edge-to-face C–H···π interactions (2.64–3.46 Å) in the type-II cavity. These multiple intermolecular interactions between C₂H₄ molecules and Np synthons were also confirmed by the Hirshfeld surface analysis of the C₂H₄ molecule within the framework (Fig. S26†), further supporting the crucial role of Np synthons in trapping C₂H₄ molecules. Moreover, the NCU-HOF1a@1.75C₂H₄ single crystal was then obtained by raising the C₂H₄ pressure to 2 bar (Table S1†). The SCXRD analysis revealed a significant increase in the number of intermolecular interactions between C₂H₄ molecules and Np synthons, accompanied by a decrease in the shortest distance of these intermolecular interactions (Fig. S27 and S28†). This is mainly ascribed to the 1.75 times increase of C₂H₄ uptake in the NCU-HOF1a@1.75C₂H₄ compared to that of NCU-HOF1a@1C₂H₄. It should be noted that the unit cells of both C₂H₄-adsorbed NCU-HOF1a single crystals remain unchanged compared to NCU-HOF1a, indicating a gradual increase in the internal rigidity of the frameworks in the order of NCU-HOF1a@1.75C₂H₄ > NCU-HOF1a@1C₂H₄ > NCU-HOF1a. Precisely, the trapped C₂H₄ molecules within the pores of C₂H₄-adsorbed NCU-HOF1a restrict the rotation of the Np synthons, reducing the nonradiative decay pathways and resulting in the fluorescence turn-up of NCU-HOF1a. This is highly consistent with the experimental data, and all of these SCXRD analyses also strongly support the preferential adsorption of C₂H₄ over C₂H₆ on NCU-HOF1a under ambient conditions.

Conclusions

In summary, we have demonstrated the facile self-correction of the hydrogen-bonding patterns in 3D NCU-HOFs, self-assembled from molecular units composed of peripheral Np hydrogen-bonded synthons and central bicarbazoles. The as-synthesized metastable NCU-HOF1 has an 11-fold interpenetrated dia topology with a quarter of the Np units exhibiting monomeric N–H···O interactions between adjacent Np link sites. These mismatched hydrogen bond patterns readily undergo an inconceivable “cross-door” rotation of nearly 180° upon desolvation, resulting in fully dimeric interactions. Consequently, the activated NCU-HOF1a becomes permanently porous with a BET surface area of 538 m² g⁻¹ and excellent robustness in highly polar solvents, strong acid, or alkaline aqueous solutions. Moreover, NCU-HOF1a demonstrates biased adsorption of C₂H₄ over C₂H₆ due to multiple C–H···O/π interactions between Np synthons and C₂H₄ guests in the contracted cavities. These host-guest interactions enhance the intramolecular rigidity of NCU-HOF1a, enabling efficient “turn-up” fluorescent sensing of C₂H₄. This work contributes to our understanding of self-correction dynamics in frameworks by nanoconfinement and their influence on the subsequent features and applications of organic porous materials.

Data availability

The data are available from the corresponding author on reasonable request.

Author contributions

H. W. proposed the research direction and guided the project. G. X. and C. Z. designed and performed the materials synthesis and characterization. X. X., F. Y., and Y. Y. took part in the discussion of experimental data and gave useful suggestions. H. W., G. X., C. Z., and X. X. drafted the manuscript. All authors discussed the results and approved the final version of the manuscript.

Conflicts of interest

There are no conflicts to declare.

Acknowledgements

This work was supported by the National Natural Science Foundation of China (No. 22063005), the Natural Science Foundation of Jiangxi Province (No. 20212ACBA203012, 20224BAB214003, 20232BAB203031), the Interdisciplinary Innovation Fund of Natural Science, Nanchang University (No. 9167-27060003-ZD2101, 9167-28220007-YB2113), and the Foundation of Jiangxi Provincial Key Laboratory of Functional Crystalline Materials Chemistry (No. 2024SSY05162).



Notes and references

- 1 R.-B. Lin, Y. B. He, P. Li, H. L. Wang, W. Zhou and B. L. Chen, *Chem. Soc. Rev.*, 2019, **48**, 1362–1389.
- 2 Z.-J. Lin, S. A. R. Mahammed, T.-F. Liu and R. Cao, *ACS Cent. Sci.*, 2022, **8**, 1589–1608.
- 3 Z. J. Zhang, Y. X. Ye, S. C. Xiang and B. L. Chen, *Acc. Chem. Res.*, 2022, **55**, 3752–3766.
- 4 S. Z. Cai, Z. F. An and W. Huang, *Adv. Funct. Mater.*, 2022, **32**, 2207145.
- 5 I. Hisaki, C. Xin, K. Takahashi and T. Nakamura, *Angew. Chem., Int. Ed.*, 2019, **58**, 11160–11170.
- 6 A. E. Amooghin, H. Sanaeepur, M. Ghomi, R. Luque, H. Garcia and B. L. Chen, *Coord. Chem. Rev.*, 2024, **505**, 215660.
- 7 J. T. Li and B. L. Chen, *Chem. Sci.*, 2024, **15**, 9874–9892.
- 8 Y. S. Yang, L. B. Li, R.-B. Lin, Y. X. Ye, Z. Z. Yao, L. Yang, F. H. Xiang, S. M. Chen, Z. J. Zhang, S. C. Xiang and B. L. Chen, *Nat. Chem.*, 2021, **13**, 933–939.
- 9 X. Zhang, L. B. Li, J.-X. Wang, H.-M. Wen, R. Krishna, H. Wu, W. Zhou, Z.-N. Chen, B. Li, G. D. Qian and B. L. Chen, *J. Am. Chem. Soc.*, 2020, **142**, 633–640.
- 10 C. H. Jiang, J.-X. Wang, D. Liu, E. Y. Wu, X.-W. Gu, X. Zhang, B. Li, B. L. Chen and G. D. Qian, *Angew. Chem., Int. Ed.*, 2024, **63**, e202404734.
- 11 S. C. Pal, D. Mukherjee, R. Sahoo, S. Mondal and M. C. Das, *ACS Energy Lett.*, 2021, **6**, 4431–4453.
- 12 Z. Y. Song, L. Miao, L. Ruhlmann, Y. K. Lv, L. C. Li, L. H. Gan and M. X. Liu, *Angew. Chem., Int. Ed.*, 2023, **61**, e202219136.
- 13 B. Han, H. L. Wang, C. M. Wang, H. Wu, W. Zhou, B. L. Chen and J. Z. Jiang, *J. Am. Chem. Soc.*, 2019, **141**, 8737–8740.
- 14 W. K. Qin, D. H. Si, Q. Yin, X. Y. Gao, Q. Q. Huang, Y. N. Feng, L. Xie, S. Zhang, X. S. Huang, T. F. Liu and R. Cao, *Angew. Chem., Int. Ed.*, 2022, **61**, e202202089.
- 15 D. Q. Yu, H. C. Zhang, Z. Q. Liu, C. Liu, X. B. Du, J. S. Ren and X. G. Qu, *Angew. Chem., Int. Ed.*, 2022, **61**, e202201485.
- 16 J. K. Tang, J. Liu, Q. Z. Zheng, W. T. Li, J. H. Sheng, L. Q. Mao and M. Wang, *Angew. Chem., Int. Ed.*, 2021, **60**, 22315–22321.
- 17 D. Q. Yu, H. C. Zhang, J. S. Ren and X. G. Qu, *Chem. Soc. Rev.*, 2023, **52**, 7504–7523.
- 18 X. Y. Song, Y. Wang, C. Wang, D. Wang, G. W. Zhuang, K. O. Kirlikovali, P. Li and O. K. Farha, *J. Am. Chem. Soc.*, 2022, **144**, 10663–10687.
- 19 R.-B. Lin and B. L. Chen, *Chem.*, 2022, **8**, 2114–2135.
- 20 P. Cui, E. S. Grape, P. R. Spackman, Y. Wu, R. Clowes, G. M. Day, A. K. Inge, M. A. Little and A. I. Cooper, *J. Am. Chem. Soc.*, 2020, **142**, 12743–12750.
- 21 Y.-L. Li, E. V. Alexandrov, Q. Yin, L. Li, Z.-B. Fang, W. B. Yuan, D. M. Proserpio and T.-F. Liu, *J. Am. Chem. Soc.*, 2020, **142**, 7218–7224.
- 22 M. Vicent-Morales, M. Esteve-Rochina, J. Calbo, E. Ortí, I. J. Vitorica-Yrezábal and G. M. Espallargas, *J. Am. Chem. Soc.*, 2022, **144**, 9074–9082.
- 23 S. Feng, Y. X. Shang, Z. K. Wang, Z. X. Kang, R. M. Wang, J. Z. Jiang, L. L. Fan, W. D. Fan, Z. N. Liu, G. D. Kong, Y. Feng, S. Q. Hu, H. L. Guo and D. F. Sun, *Angew. Chem., Int. Ed.*, 2020, **59**, 3840–3845.
- 24 H. L. Wang, B. Li, H. Wu, T.-L. Hu, Z. Z. Yao, W. Zhou, S. C. Xiang and B. L. Chen, *J. Am. Chem. Soc.*, 2015, **137**, 9963–9970.
- 25 T.-H. Chen, I. Popov, W. Kaveevivitchai, Y.-C. Chuang, Y.-S. Chen, O. Daugulis, A. J. Jacobson and O. S. Miljanic, *Nat. Commun.*, 2014, **5**, 5131.
- 26 M. I. Hashim, H. T. M. Le, T.-H. Chen, Y.-S. Chen, O. Daugulis, C.-W. Hsu, A. J. Jacobson, W. Kaveevivitchai, X. Liang, T. Makarenko, O. S. Miljanic, I. Popovs, H. V. Tran, X. Q. Wang, C.-H. Wu and J. I. Wu, *J. Am. Chem. Soc.*, 2018, **140**, 6014–6026.
- 27 W. Q. Yan, X. P. Yu, T. Yan, D. F. Wu, E. L. Ning, Y. Qi, Y.-F. Han and Q. W. Li, *Chem. Commun.*, 2017, **53**, 3677–3680.
- 28 A. Maurya, K. Marvaniya, P. Dobariya, M. V. Mane, S. Tothadi, K. Patel and S. Kushwaha, *Small*, 2023, 2306824.
- 29 A. Pulido, L. J. Chen, T. Kaczorowski, D. Holden, M. A. Little, S. Y. Chong, B. J. Slater, D. P. McMahon, B. Bonillo, C. J. Stackhouse, A. Stephenson, C. M. Kane, R. Clowes, T. Hasell, A. I. Cooper and G. M. Day, *Nature*, 2017, **543**, 657–664.
- 30 M. Mastalerz and I. M. Oppel, *Angew. Chem., Int. Ed.*, 2012, **51**, 5252–5255.
- 31 X.-Y. Chen, L.-H. Cao, X.-T. Bai and X.-J. Cao, *Chem. Eur. J.*, 2024, **30**, e202303580.
- 32 A. Karmakar, R. Illathvalappil, B. Anothumakkol, A. Sen, P. Samanta, A. V. Desai, S. Kurungot and S. K. Ghosh, *Angew. Chem. Int. Ed.*, 2016, **55**, 10667.
- 33 Y. Y. Sun, J. Wei, Z. H. Fu, M. Y. Zhang, S. G. Zhao, G. Xu, C. S. Li, J. Zhang and T. H. Zhou, *Adv. Mater.*, 2023, **35**, 2208625.
- 34 G. R. Desiraju, *Angew. Chem., Int. Ed. Engl.*, 1995, **34**, 2311–2327.
- 35 M. A. Little and A. I. Cooper, *Adv. Funct. Mater.*, 2020, **30**, 1909842.
- 36 B. Wang, R.-B. Lin, Z. J. Zhang, S. C. Xiang and B. L. Chen, *J. Am. Chem. Soc.*, 2020, **142**, 14399–14416.
- 37 Q. Zhu, L. Wei, C. Zhao, H. X. Qu, B. W. Liu, T. Fellowes, S. Y. Yang, A. Longcake, M. J. Hall, M. R. Probert, Y. B. Zhao, A. I. Cooper and M. A. Little, *J. Am. Chem. Soc.*, 2023, **145**, 23352–23360.
- 38 S. M. Chen, Y. Ju, Y. S. Yang, F. H. Xiang, Z. Z. Yao, H. Zhang, Y. B. Li, Y. F. Zhang, S. C. Xiang, B. L. Chen and Z. J. Zhang, *Nat. Commun.*, 2024, **15**, 298.
- 39 S. C. Wang, Q. S. Zhang, Z. Wang, S. Q. Guan, X. D. Zhang, X. H. Xiong and M. Pan, *Angew. Chem., Int. Ed.*, 2023, **62**, e202315382.
- 40 D. Wang and Y. Zhao, *Angew. Chem., Int. Ed.*, 2023, **62**, e202217903.
- 41 J. C. Jiang, Y. B. Zhao and O. M. Yaghi, *J. Am. Chem. Soc.*, 2016, **138**, 3255–3265.
- 42 A. K. Mohammed, J. Raya, A. Pandikassala, M. A. Addicoat, S. Gaber, M. Aslam, L. Ali, S. Kurungot and D. Shetty, *Angew. Chem. Int. Ed.*, 2023, **62**, e202304313.



43 T. Hashimoto, R. Oketani, M. Nobuoka, S. Seki and I. Hisaki, *Angew. Chem., Int. Ed.*, 2023, **62**, e202215836.

44 X. Yang, J. Huang, S. Y. Gao, Y. Q. Zhao, T. Huang, H. F. Li, T. F. Liu, Z. Y. Yu and R. Cao, *Adv. Mater.*, 2023, **35**, 2305344.

45 F. L. Hu, C. P. Liu, M. Y. Wu, J. D. Pang, F. L. Jiang, D. Q. Yuan and M. C. Hong, *Angew. Chem., Int. Ed.*, 2017, **56**, 2101–2104.

46 M. A. Rahman, C. J. Dionne and A. Giri, *Nano Lett.*, 2022, **22**, 8534–8540.

47 J. K. Gao, Y. L. Cai, X. F. Qian, P. X. Liu, H. Wu, W. Zhou, D.-X. Liu, L. B. Li, R.-B. Lin and B. L. Chen, *Angew. Chem., Int. Ed.*, 2021, **60**, 20400–20406.

48 P. H. Li, P. Li, M. R. Ryder, Z. C. Liu, C. L. Stern, O. K. Farha and J. F. Stoddart, *Angew. Chem., Int. Ed.*, 2019, **58**, 1664–1669.

49 Q. Ji, K. Takahashi, S.-I. Noro, Y. Ishigaki, K. Kokado, T. Nakamura and I. Hisaki, *Cryst. Growth Des.*, 2021, **21**, 4656–4664.

50 Y. Z. Zhou, C. Chen, R. Krishna, Z. Y. Ji, D. Q. Yuan and M. Y. Wu, *Angew. Chem., Int. Ed.*, 2023, **62**, e202305041.

51 X. J. Ding, Z. Y. Liu, Y. S. Zhang, G. Ye, J. F. Jia and J. Chen, *Angew. Chem., Int. Ed.*, 2022, **61**, e202116483.

52 B. Q. Yu, S. B. Geng, H. L. Wang, W. Zhou, Z. J. Zhang, B. L. Chen and J. Z. Jiang, *Angew. Chem., Int. Ed.*, 2021, **60**, 25942–25948.

53 Y. Lv, J. Liang, Z. Xiong, H. Zhang, D. Li, X. Yang, S. Xiang and Z. Zhang, *Chem.-Eur. J.*, 2023, **29**, e202204045.

54 Y. L. Cai, J. K. Gao, J.-H. Li, P. X. Liu, Y. C. Zheng, W. Zhou, H. Wu, L. B. Li, R.-B. Lin and B. L. Chen, *Angew. Chem., Int. Ed.*, 2023, **62**, e202308579.

55 Y. Wang, K. Ma, J. Q. Bai, T. Xu, W. D. Han, C. Wang, Z. X. Chen, K. O. Kirlikovali, P. Li, J. S. Xiao and O. K. Farha, *Angew. Chem., Int. Ed.*, 2022, **61**, e202115956.

56 Y. Suzuki, N. Tohnai, A. Saeki and I. Hisaki, *Chem. Commun.*, 2020, **56**, 13369–13372.

57 G. G. Ye, Y. G. Wang, L. M. Hong, F. Q. Yu, G. M. Xia and H. M. Wang, *J. Mater. Chem. C.*, 2021, **9**, 9142–9146.

58 C. L. Zhou, M. D. Wang, W. H. Guo, G. G. Ye, Y. G. Wang, Y. Yang, G. M. Xia and H. M. Wang, *Dyes Pigm.*, 2023, **213**, 111198.

59 A. L. Spek, *J. Appl. Crystallogr.*, 2003, **36**, 7–13.

60 W. Yang, J. W. Wang, H. L. Wang, Z. B. Bao, J. C.-G. Zhao and B. L. Chen, *Cryst. Growth Des.*, 2017, **17**, 6132–6137.

61 D. Sengupta, P. Melix, S. Bose, J. Duncan, X. J. Wang, M. R. Mian, K. O. Kirlikovali, F. Joodaki, T. Islamoglu, T. Yildirim, R. Q. Snurr and O. K. Farha, *J. Am. Chem. Soc.*, 2023, **145**, 20492–20502.

